On the Hybrid Kinematics of Tethered Mobile Robots

Michael A. Sebok and Herbert G. Tanner

Abstract— **Tethered mobile robots have for a long time been utilized in search and rescue and deployment in inaccessible or hazardous environments. From inspection and cleanup inside nuclear waste tanks to underwater inspection, tethers and umbilical cords have been a reliable means of uninterrupted power supply, high-bandwidth communication, and means of either deployment or recovery in cases of system failure. While typically tethered robots have been teleoperated, this is not necessarily the case, and this paper is concerned with aspects of tether monitoring and management which are central to autonomous operations. Specifically, the paper reports on a method to approximate tether shape and configuration in cluttered workspaces for mobile robots equipped with spooling mechanisms capable of releasing or collecting a cable of which the free end is fixed in the workspace.**

I. INTRODUCTION

Robotic systems occasionally utilize tethered connections to their environment or other systems as a means of increasing their mobility (Fig. 1), stability, or functionality [1]–[5]. A tether on a mobile robot can support weight, provide power, facilitate communication, and offer reliable means of physical extraction from a cluttered environment in case of failure. While tethers can in general increase the capability of a system, they often pose a new set of constraints on the system dynamics, complicate motion planning and inter-robot interaction coordination plans —especially in cluttered spaces— and make imperative the accurate modeling and analysis of the interaction between robot, tether, and environment.

(a) (b)

Fig. 1: Custom-built, spool-equipped mobile robots with increased mobility characteristics. (a) Tether-assisted ascent over a fence; (b) Tether-enabled controlled descent from the ceiling.

Sebok and Tanner are with the Department of Mechanical Engineering, University of Delaware, Newark, DE 19716 USA {sebokm,btanner}@udel.edu

While the planning of the motion of robots on a tether could benefit from a simple, yet reasonably accurate model that can predict the configuration of the tether given the history of motion of the tethered vehicle, not enough attention has been paid on deriving such models. For instance, a system which tracks tether or umbilical cord configuration in search and rescue missions and could predict entanglements would certainly facilitate operators [1], while requiring less manpower and allowing for a faster and more reliable response. Additionally, it would provide better prediction of robot location and penetration in the absence of maps, GPS, or localization infrastructure.

Tethers have also been utilized for cooperation and direct interaction between vehicles in multi-robot systems [2], [3]. While umbilical cords can allow power sharing between vehicles [3], passive mechanical connections between vehicles through tether interaction can offer unique new mobility features, such as enabling controlled cooperative vertical ascent or descent [2]. When tethers are taut [2], [4], dynamical modeling and kinematic simulation have their own challenges but are conceptually straightforward; when the tethers are not [1], [3], however, it is not clear what kind of analytically amenable tether kinematics models can inform a high-level robot motion planner or controller.

Motion planning involving tethers or other types of deformable material capable of exerting forces on a robotic device is not an entirely new idea [6]. In fact, the actual problem of planning fixed-length tether configurations in cluttered planar environments has been approached as a discrete (graph) search problem, using homotropic classes of curves as primitives [5]. Looking at the tether in isolation, however, may not always be appropriate in applications involving tethered mobile robots, as it ignores the role of the tethered vehicle in affecting the state and shaping the form of the tether itself.

Furthermore, the ability to predict and affect tether configuration can provide insights and open new opportunities in human-robot interaction applications [4]. One very specific application area of particular interest in the context of physical interaction between machines and humans is found in the area of early pediatric (infant) motor rehabilitation using harness systems [7], [8]. Existing systems of this nature are currently passive in terms of the physical interaction between the child and the harness system itself, with the latter serving merely in the role of a reconfigurable gravity-assistance device. It is conceivable, however, such cable-driven harness systems can be instrumented, be semi-automated, and become components of an *adaptive* system for (human) motor rehabilitation.

This paper describes a novel method for approximating the tether shape and configuration when a tethered mobile robot moves in a cluttered environment. The method draws from elements of workspace modeling and mathematical representation that are used in motion planning methods based on navigation functions [9], [10]. Assuming that the robot can physically interact with its environment and can utilize the tether for ascent or descent (Fig. 1), a hybrid system can be defined to describe the kinematics of the robot in different modes of operation. The guards that regulate the transitions in this hybrid system depend on knowledge of the tether's configuration. The thesis of this paper, therefore, is that analytically and computationally tractable ways of predicting tether configuration can decisively contribute to the simulation and motion planning for such systems.

The remaining portion of the paper is organized in the following way. Section II introduces the formal mathematical formulation of the tethered crawler problem. Section III constructs the model of the crawler as well as the tether transformation. Section IV reviews the simulation of the inverse purging transformation and the resulting tethered crawler kinematics. Section V discusses the relative advantages and disadvantages of the given methodology. Finally, Section VI summarizes the key results of the work.

II. Problem Statement

Consider a tethered wheeled mobile robot moving on a vertical two-dimensional plane $Q \subset \mathbb{R}^2$, constrained by obstacles and under the effect of gravity (Fig. 2). The robot's coordinates are denoted as a pair $q = (x, y)$. One end of the tether is attached to the robot, and the other is fixed at an anchoring location $(x_a, y_a) \in Q$ in the workspace. The robot is assumed to have a powered spool to allow it to pull or release the tether at will; pulling the tether exerts a force on the robot, which can be used to overcome workspace obstacles, and reach a desired configuration $(x_g, y_g) \in Q$. Both robot and tether are assumed to have mass.

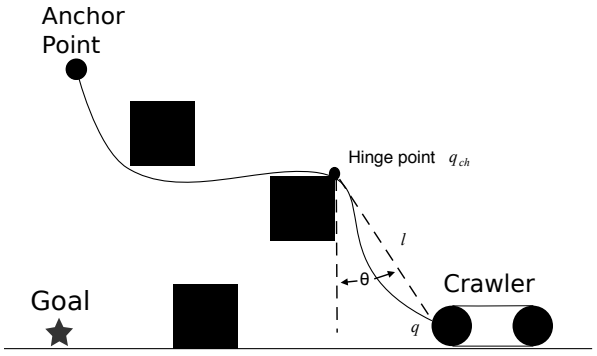

Fig. 2: A two-dimensional scenario where a tethered robot needs to utilize its tether to negotiate obstacles.

In the context of this problem, the robot is allowed to come in contact with the workspace boundary, and exploit this interaction if possible to reach its goal configuration. The workspace is populated by n obstacles, each with implicit representation in the form of a function $\beta_i : Q \to \mathbb{R}$, for $i \in \{1, \ldots, n\}$, assuming negative values in the interior of the obstacles, vanishing on their boundary, and increasing as the distance between q and the obstacle boundary increases.

The tethered robot uses its powered spool to reel in its tether while moving toward the anchor point, and releasing it while moving away, so that the line does not accumulate on the ground or gets tangled. While the robot moves on a horizontal surface and the tether has enough length, the tether lays ahead of the robot without tension (Fig. 3 top); when the tether becomes taut, it exerts a force on the robot which can lift it off the ground (Fig. 3 bottom).

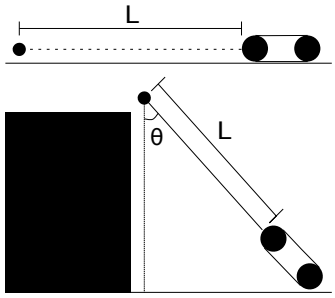

Fig. 3: Top: The robot moving horizontally without interacting kinetically with the tether. Bottom: The robot swinging from a hinge point at the top of an obstacle.

III. Technical Approach

A. Workspace topology modeling

The topology of the free space in Q is captured analytically in the form of a navigation function φ [10], a scalar function ranging from zero to one, being uniformly maximal on the boundary and having a single minimum at the goal location. A function that quantifies the distance-to-goal is denoted $\gamma(x, y)$ and could be defined as simply as the squared norm of the difference between (x, y) and the goal coordinates. The workspace is populated with M internal obstacles, each with internal representation $\beta_i(x, y) : Q \to \mathbb{R}$ for $i = \{1, \ldots, M\}$. A function β_i assumes negative values in the interior of obstacle i, vanishes on the boundary, and monotonically increases as the distance from the obstacle boundary increases. The exterior boundary of the workspace is outlined via function β_0. Space limitations do not permit a detailed presentation of the construction of φ, which involves a star-to-sphere diffeomorphic transformation h of the interior obstacles and the boundary, parameterized by a positive constant λ. If the obstacles are not star-shaped, but can instead be expressed as trees of partially overlapping stars, then a *purging transformation* f_μ is utilized to transform the boundary of each outer branch of one of those trees onto the boundary of its parent branch iteratively, until the final remaining region is star-shaped. This latter construction is borrowed and re-purposed for modeling of the tether configuration in the following section.

B. Tether modeling

In both modes of Fig. 3, the motion of the tethered robot will be approximated with that of a (rigid) pendulum of

varying length, where all the mass is lumped at the end point. The lumped mass has no elasticity, so when it collides with the workspace boundary, it does not rebound. In an unobstructed region of the plane Q, and if all tether slack has been reeled in, the robot will swing about a hinge point (x_h, y_h); if no obstacles are present, this hinge point will be the anchor point (x_a, y_a). If there are obstacles, however, and the tether lays on top of them, then there may be a multitude of such hinge points, located on the edge of the obstacles (Fig. 2). Let the number of possible hinge points be m and denote Q_h the set of all those points, including (x_a, y_a). To approximate the tether configuration, the mathematical machinery put in place to construct the navigation function φ is utilized for this purpose. It has been shown [9] that a diffeomorphic transformation that maps star trees into spheres as part of the navigation function construction, can be "pushed" all the way to collapse interior obstacle boundaries into *points*. If this diffeomorphism Φ is applied, a straight line segment $\Lambda(s) = q_1(1-s) + q_2\, s$, $s \in [0,1]$, connecting the two ends of the tether say q_1 and q_2, in the transformed workspace will generate a path in the original space via Φ^{-1} which has probability zero to intersect with obstacles.

The argument now is that it is not critical that $\Phi^{-1}(\Lambda)$ does not match exactly the actual shape of the tether. What is important from the planner's viewpoint is to identify the high curvature locations, as these could potentially be associated with hinge points for the tethered platform. To this end, the workspace modeling mathematical infrastructure put in place in Section III-A is being adapted and reused for predicting the shape of the tether. Specifically, the diffeomorphic transformation Φ is reconstructed in a form Φ_δ by replacing $\gamma(x,y)$ with $\delta(q) \triangleq ||q - q_1|| \cdot ||q - q_2||$. The rest of the construction remains intact; the end result is a diffeomorphism, the inverse of which maps an arbitrary path (line segments included) in the point-space to a curve that meanders between the obstacles. Minimal knowledge of how the actual tether is threaded through the workspace, e.g. which side of an obstacle it passes around, is sufficient for approximating the shape of the tether in the original star-world workspace. Choices for the path drawn in point space include a line segment connecting q_1 to q_2, or a series of segments connecting these two end points to obstacle points in between. The focus of this particular paper is not on exploration of these possibilities or the identification of the one that yields the most accurate approximation. Instead, the emphasis here is in formulating a hybrid system model for the tethered platform which can be informed by such approximations, and indicating one avenue of investigation for generating such approximations.

Irrespectively of the choice of this original curve $\Lambda(s)$, the inverse transformation $\Phi_\delta^{-1}(\Lambda)$ yields a tether shape approximation. Typically, no closed form, analytical expression for this inverse transformation would be available. Given, however, that Φ_δ is a diffeomorphism, a numerical approximation in the form

$$\Phi_\delta^{-1}(x + \delta x) \approx \Phi_\delta^{-1}(x) + \nabla\Phi_\delta^{-1}(x)\,\Delta x$$

usually suffices. Now the extrema of the *derivative* of this inverse transformation $\nabla\Phi_\delta^{-1}$ reveals locations along the tether that can be potential hinge points; with the choice of a threshold $\tau > 0$, the hinge point set Q_h is populated as follows

$$Q_h = \{(x_h, y_h) : \|\nabla\Phi_\delta^{-1}(x_h)\| > \tau\} \cup \{(x_a, y_a)\}$$

C. Hybrid robot dynamics

Taking into account the aforementioned model of the tether, the different modes of mobility for the robot are modeled as variable-length pendulum motion. The robot at the end of the tether is able to move along some surfaces[1] without tether action. Otherwise, the robot moves along a boundary by reeling the tether or swings freely from the current hinge point until impacting a surface. As it undergoes transitions between these modes, the vehicle dynamics are represented in the form of a *hybrid automaton* [11]. Specifically, this is a tuple $\langle L, X, A, W, E, \mathrm{Inv}, \mathrm{Act}\rangle$ with components:

L	a finite set of locations;[(i)]
X	the continuous state space;
A	a finite set of labels;[(ii)]
W	the continuous communication space;[(iii)]
E	a finite set of events;[(iv)]
Inv	the invariants of continuous dynamics;[(v)]
Act	the assignment of continuous dynamics;[(vi)]

[(i)] the nodes in the hybrid automaton graph (Fig. 4);
[(ii)] the discrete input alphabet that trigger transitions in the automaton's graph and label its edges (Fig. 4);
[(iii)] the domain of external variables that affect its behavior, e.g. control inputs;
[(iv)] the automaton's transitions (Fig. 4), in the form of tuples $\langle$initial location, action, guard condition, resets on continuous variables, new location$\rangle$;
[(v)] the subsets of X, one for every $\ell \in L$ which remain invariant under the dynamics imposed by $\mathrm{Act}(\ell)$.
[(vi)] the function that assigns a set of differential equations to each location.

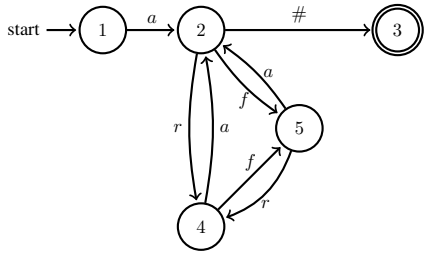

Fig. 4: Automaton graph for a tethered wheeled robot.

The components of the hybrid automaton are for the particular case of the mobile robot of Section II, the graph of which is shown in Fig. 4, are defined in more detail below.

[1]Assumed here straight, for simplicity.

The continuous states of the system are four: the position and velocity of the mobile robot in the plane of motion and their associated derivatives. The association of the dynamics of this system to that of a pendulum with variable length motivates a polar parameterization that involves *length* and *angle*, relative to the closest tether hinge point. The continuous state space therefore is defined as $X = \mathbb{R}_+ \times \mathrm{S} \times \mathbb{R}^2$, with $x = (l, \theta, \dot{l}, \dot{\theta}) \in X$.

Note, however, that mapping (l, θ) to (x, y) is not possible without knowledge of the current hinge point (x_h, y_h); see Fig. 2—(l, θ) are relative coordinates. Hinge point locations are treated as *communication variables* for this system. The two continuous communication variables thus form a pair $(x_h, y_h) \in Q_h$ (see Section III-B) and express the absolute coordinates of the tether hinge point that affects the motion of the robot. The other exogenous to the system signal that plays a role in its evolution is the robot's (bounded) control input $u \in [-u_{\mathsf{max}}, u_{\mathsf{max}}] \subset \mathbb{R}$. Therefore, $W \subseteq Q_h \times [-u_{\mathsf{max}}, u_{\mathsf{max}}]$.

The *label* set consists of three symbols: $A = \{a, r, f\}$. Label a represents horizontal motion on a flat surface where the tether exerts no tensile force on the robot. Label r is for tether-assisted motion where the tether is being reeled, and label f is associated with free-swinging from a hinge point until impact. Symbol $\#$ is not formally part of the label set, but it marks a transition to a final state.

There are five discrete *locations*: $L = \{1, 2, 3, 4, 5\}$. Locations 1 and 3 correspond to initial and final states in the automaton, transitions to which are not explicitly labeled. Each one of the other locations is associated with a group of continuous states that belong to the positive limit set of the dynamics of the system that are triggered by events labeled by A. Location 1 corresponds to the mode of operation where the robot rolls on a surface without being subjected to a tension force by the tether; the latter is being reeled in without being taut. Location 4 is one where the robot is leveraging the tether tension for controlled ascent or descent under gravity, and location 5 is associated to a condition where the robot swings from a hinge point without having contact with any surface.

The automaton's transitions are (forcibly) triggered by *guards*, denoted G_ℓ with $\ell \in A$ and expressed in terms of equality or inequality constraints involving continuous states and communication variables—latter being control input u and *current* hinge point $q_{hc} = \arg\min_{Q_h} \|q - q_h\|$, i.e. the member of Q_h with the smallest Euclidean distance to (x, y). The value of the navigation function φ is used as an indicator for proximity to workspace boundary; if $\varphi(x, y) \geq c < 1$ where c is a threshold, then it is understood that the robot is in contact with the free workspace boundary. The robot can move unassisted by the tether whenever it has enough actuator authority to overcome gravity (its acceleration $\vec{g}$):

$$\left\| m\,\vec{g} \times \frac{\nabla\varphi}{\|\nabla\varphi\|} \right\| \triangleq u_c < u_{\mathsf{max}}$$

The guards are parameterized with the current hinge point q_{hc}, available as a communication variable and which in conjunction to (l, θ) can determine (x, y):

$$G_a^{q_{hc}} = \{(l,\theta) \in Q \mid \dot{\theta} = 0,\ \varphi(x,y) \geq c,\ |u| < u_c(x,y)\}$$
$$G_r^{q_{hc}} = \{(l,\theta) \in Q \mid \dot{\theta} = 0,\ \varphi(x,y) \geq c,\ |u| > u_c(x,y)\}$$
$$G_f^{q_{hc}} = \{(l,\theta) \in Q \mid \dot{\theta} \neq 0,\ \varphi(x,y) < c,\ |u| \geq u_c(x,y)\}$$
$$G_\#^{q_{hc}} = \{(l,\theta) \in Q \mid \varphi(x,y) < 1 - c\}$$

Transitions out of locations 2, 4, and 5 induce resets on the continuous states and communication variables (hinge point locations)—the latter being the result of the robot reeling in the tether and reducing its length. In effect, as soon as $\|q - q_h\| \to 0$ for a $q_h \in Q_h$, this hinge point disappears. For transitions that do not affect an instantaneous change in the state, the state and communication variables map to the current hinge point q_{hc}, tether length l_c, and tether angle θ_c. Resets are captured as instantaneous mappings, or *jumps*, denoted J and indexed by the event that triggers them.

$$J_{(1,2)} : \begin{cases} Q_h \mapsto \{q_{hc}\} \\ l \mapsto \{l_c\} \\ \theta \mapsto \{\theta_c\} \end{cases}$$
$$J_{(2,4)} : \begin{cases} Q_h \mapsto Q_h \setminus \{q_{hc}\} \\ l \mapsto \min_{Q_h \setminus \{q_{hc}\}} \|q_h - q\| \\ \theta \mapsto \arcsin \vec{g} \times \frac{\arg\min_{Q_h \setminus \{q_{hc}\}} \|q_h - q\| - q}{g \min_{Q_h \setminus \{q_{hc}\}} \|q_h - q\|} - \frac{\pi}{2} \end{cases}$$
$$J_{(5,4)} = J_{(4,5)} = J_{(1,2)}$$
$$J_{(2,5)} = J_{(4,2)} = J_{(5,2)} = J_{(2,4)}$$

With the guards and jump maps in place, the automaton's *events* can be defined as follows. As indicated, events take the form of a tuple, and for the eight transitions shown in Fig. 4, the events are written as

$$E_1 = \langle 1, a, G_a^{q_{hc}}, J_{(1,2)}, 2\rangle \quad E_2 = \langle 2, r, G_r^{q_{hc}}, J_{(2,4)}, 4\rangle$$
$$E_3 = \langle 2, f, G_f^{q_{hc}}, J_{(2,5)}, 5\rangle \quad E_4 = \langle 4, a, G_a^{q_{hc}}, J_{(4,2)}, 2\rangle$$
$$E_5 = \langle 4, f, G_f^{q_{hc}}, J_{(4,5)}, 5\rangle \quad E_6 = \langle 5, a, G_a^{q_{hc}}, J_{(5,2)}, 2\rangle$$
$$E_7 = \langle 5, r, G_r^{q_{hc}}, J_{(5,4)}, 4\rangle \quad E_8 = \langle 2, \#, G_\#^{q_{hc}}, J_{(1,2)}, 3\rangle$$

Locations $\ell \in L$ have each their own *invariant* $\mathrm{Inv}_{(\ell)}^{q_{hc}}$, parameterized by the current hinge point q_{hc}, similarly to guards. An invariant is a region in X where the continuous state and communication variables lie for as long as the automaton is at the particular location. When the state exits any one of these invariants, the guards and events designate a transition to a new location. For the system at hand, the invariants are specified as follows.

$$\mathrm{Inv}_{(1)}^{q_h} = \{(l,\theta) \in X \mid \dot{\theta} = \dot{l} = 0,\ \varphi(x,y) \geq c\}$$
$$\mathrm{Inv}_{(2)}^{q_h} = \{(l,\theta) \in X \mid \dot{\theta} = 0,\ \varphi(x,y) \geq c,\ |u| < u_c(x,y)\}$$
$$\mathrm{Inv}_{(3)}^{q_h} = \{(l,\theta) \in X \mid \dot{\theta} = \dot{l} = 0,\ \varphi(x,y) < 1 - c\}$$
$$\mathrm{Inv}_{(4)}^{q_h} = \{(l,\theta) \in X \mid \dot{\theta} = 0,\ \varphi(x,y) \geq c,\ |u| > u_c(x,y)\}$$
$$\mathrm{Inv}_{(5)}^{q_h} = \{(l,\theta) \in X \mid \dot{\theta} \neq 0,\ \varphi(x,y) < c,\ |u| \geq u_c(x,y)\}$$

The continuous dynamics are determined for each location by the *assignment map* $\mathrm{Act} : L \to TX$ (the tangent space of

X). In what follows, T denotes tether tension, m stands for the mass of the robot, u is the robot's input, and $\delta(q)$ stands for the Dirac delta function. The latter is utilized to capture the effect of impact of the robot to workspace boundaries. The assignment maps are as follows.

$$\text{Act}(i) = \begin{cases} \ddot{l} = -g\cos(\theta) + T + \frac{u}{m} \\ \ddot{\theta} = 0 \end{cases} \quad \text{for } i \in \{1, \ldots, 4\}$$

$$\text{Act}(5) = \begin{cases} \ddot{l} = -g\cos(\theta) + T - \dot{l}\delta(t) + \frac{u}{m} \\ \ddot{\theta} = -\frac{g}{l}\sin(\theta) - \frac{2i\dot{\theta}}{l} - l\dot{\theta}\delta(t) \end{cases}$$

IV. Numerical Validation

A. Simulation setup

Consider a simple scenario in which the mobile robot has to climb over a vertical wall—similarly to the case depicted in Fig. 1a. The objective here is to test the capacity of the reported method to simulate kinematically the behavior of the robot as it utilizes its tether, the latter anchored to a point on the other side of the wall and connected to a powered spool on the robot's body, to climb over this wall (see Fig. 5a). The first step in the process is to predict the shape of the tether, and identify the locations along the cable line that could act as hinge points.

B. Hinge Point Determination

Assume that the fixed anchor point for the tether is located at coordinates $(x, y) = (-0.5, 0)$ (all lengths assumed in meters), and the mobile robot's spool is initially at the point with coordinates $(0.75, -0.75)$ (Fig. 5a). The ground forms a workspace boundary along the plane where $x = -1$, while the vertical wall is an obstacle in the shape of a thin rectangle centered at $x = 0$, and extending up to $y = 0$ (see Fig. 5a).

The methodology predicts the emergence of three successive hinge points (Fig. 5c). With the robot moving to the right approaching the wall, the prediction is that point 1 will first serve as a hinge point, triggering a swing behavior for the robot as it reels in its tether until it hits the vertical wall. A second hinge point at location 2 is identified for the portion of the motion of the robot as it goes over the edge, after which the last hinge point at location 3 will be the tether's fixed anchor.

C. Simulating tethered robot motion

With these hinge points (Fig. 5c) the kinematics of the robot is simulated as it attempts to reach the left side of the wall in Fig. 5a. The robot kinematics assume a constant acceleration induced by the tether in the direction of the first hinge point in front of the robot along the curve defined by the tether.

Figure 6 illustrates the result of simulating the robot's maneuver, and Fig. 7 provides some insight into the transition between phases II and III, the former corresponding to free swinging in pendulum motion until it hits the wall, at which point it transitions to tether-enabled vertical climb along the side of the wall. The robot undergoes five distinct phases, labeled by uppercase roman numerals in Fig. 6, each

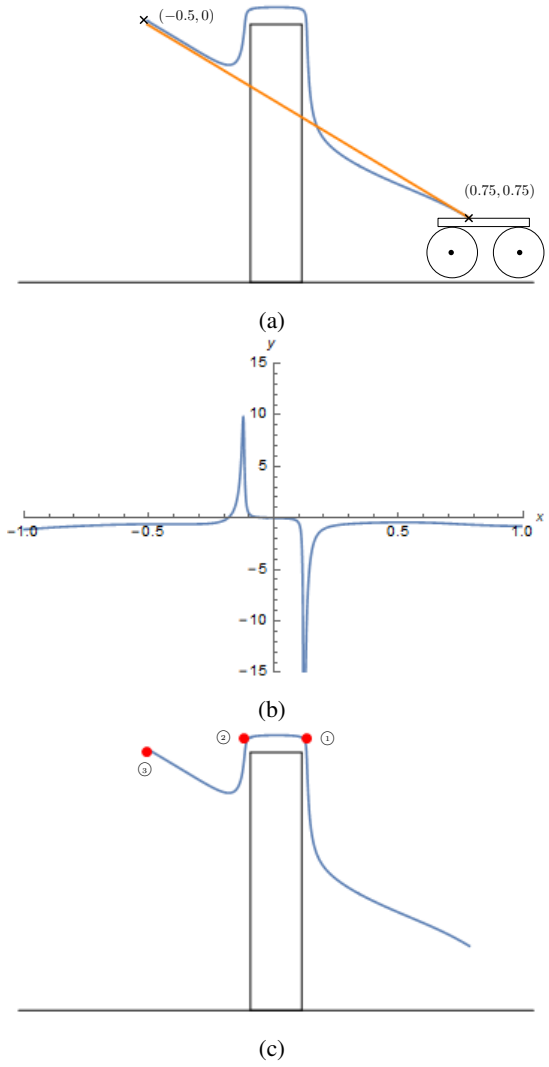

Fig. 5: (a) The inverse transform of a straight line between spool and anchor point produces an estimate of the tether configuration as dropped over the wall. (b) Curvature along the approximated tether configuration. (c) Identification of potential hinge points on the tether, informed by the spikes observed in the curvature of the approximated tether path.

corresponding to different dynamics, and with transitions between them dictated by the relative position between robot, hinge point set, and workspace boundary.

V. Discussion

The main advantage of the reported methodology is that it obviates the need for high-fidelity (e.g. finite-element based) models for the deformable cable in order to estimate its configuration and inform on the succession of the robot's kinematic modes. As it turns out, the critical elements that determine the transition between these modes in relatively simple situations as the ones analyzed and reported in this paper, are (a) the topology of the workspace which is assumed known, and (b) the location of tether points in the neighborhood of which the combined robot-tether system can behave as a pendulum. Once the tethered robot is represented mathematically in the form of a hybrid system, knowledge of

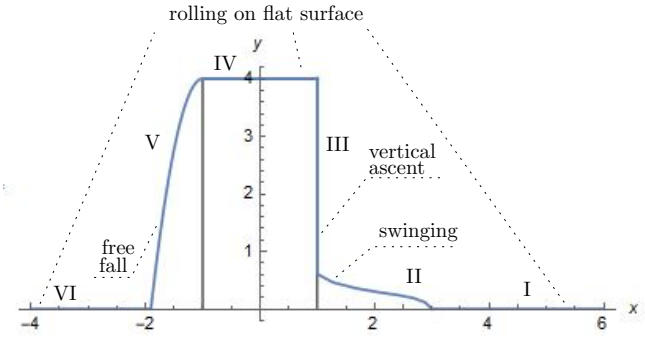

Fig. 6: Path of the robot during the wall climbing maneuver and the different phases of motion. (I) rolling toward the wall; (II) pendulum motion from hinge point ①; (III) rolling on top of the wall; (IV) free fall off the wall; (V) rolling away from the wall.

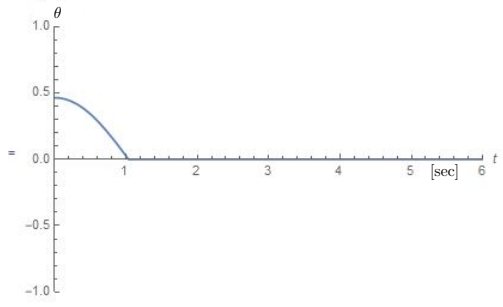

(a)

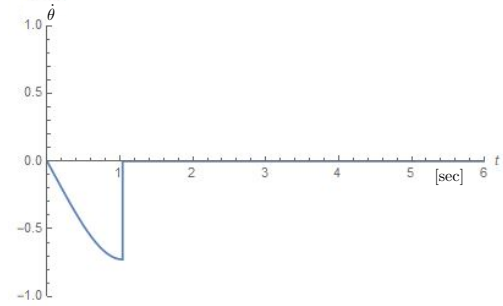

(b)

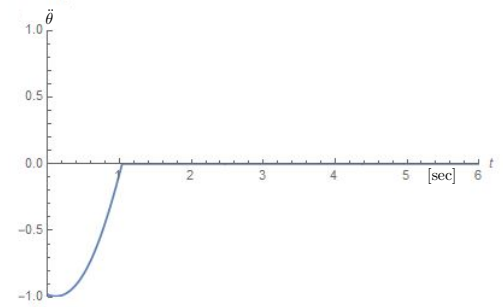

(c)

Fig. 7: Pre- and post-impact to wall simulation results. (a) Time evolution of the angle θ of the pendulum formed between the robot and the hinge point ① once the robot loses contact with the ground; just after the first simulation second, the robot hits the vertical wall and starts climbing up as it reels in its tether. (b) History of $\dot{\theta}$ during this transition. (c) angular acceleration.

these elements can allow a fairly accurate and fast simulation of the system's kinematics, without resorting to PDE solvers.

The analysis presented here is only a first step in this direction; it remains to be extended and tested in higher-dimensional spaces and more complex cluttered environments. In addition, preliminary analysis indicated the appearance of *transient* hinge points during motion where there is no contact between the robot and the workspace boundaries (ground, walls, etc.) Such phenomena occur for instance when the tether wraps around an object while the robot swings, causing a sudden, temporary shortening of the active tether length.

VI. Conclusion

While untethered robotic devices are appealing in terms of autonomy, tethers and umbilical cords have their role in robot deployments, especially in unknown and adversarial environments. In fact, they can enhance the mobility capabilities of the platforms utilizing them, allowing them new modes of operation, but they bring analysis challenges of their own, as the motion of tethered robots can ultimately depend on the configuration of the tether. Under the right assumptions, it is possible for this configuration to be approximated to the degree that the tether's effect on the vehicle motion behavior can be accurately predicted. The methodology reported in this paper is a step in the direction of incorporating such information in high-level motion planners for tethered robots.

References

[1] J. Casper and R. Murphy, "Human-robot interactions during the robot-assisted urban search and rescue response at the World Trade Center," *IEEE Transactions on Systems, Man, and Cybernetics, Part B (Cybernetics)*, vol. 33, no. 3, pp. 367–385, 2003.

[2] P. Pirjanian, C. Leger, E. Mumm, B. Kennedy, M. Garrett, H. Aghazarian, S. Fanitor, and P. Schenker, "Distributed control for a modular, reconfigurable cliff robot," in *Proceedings of the IEEE International Conference on Robotics and Automation*, 2002, pp. 4083–4088.

[3] C. Papachristos and A. Tzes, "The power-tethered UAV-UGV team: a collaborative strategy for navigation in partially-mapped environments," in *Proceedings of the 22nd Mediterranean Conference on Control and Automation*, pp. 1153–1158.

[4] S. Lupashin and R. D'Andrea, "Stabilization of a flying vehicle on a taut tether using inertial sensing," *2013 IEEE/RSJ International Conference on Intelligent Robots and Systems*, pp. 2432–2438, 2013.

[5] S. Kim, S. Bhattacharya, and V. Kumar, "Path planning for a tethered mobile robot," in *Proceedings of the 2014 IEEE International Conference on Robotics and Automation*, pp. 1132–1139.

[6] H. G. Tanner, S. G. Loizou, and K. J. Kyriakopoulos, "Nonholonomic navigation and control of cooperating mobile manipulators," *IEEE Transactions on Robotics and Automation*, vol. 19, no. 1, pp. 53–64, Feb 2003.

[7] A. Zehfroosh, E. Kokkoni, H. G. Tanner, and J. Heinz, "Learning models of human-robot interaction from small data," in *Proceedings of the 25th IEEE Mediterranean Conference on Control and Automation*, 2017, pp. 223–228.

[8] E. Kokkoni, S. W. Logan, T. Stoner, T. Peffley, and J. C. Galloway, "Use of an In-home Body Weight Support System by a Child with Spina Bifida," *Pediatric Physical Therapy*, vol. 00, pp. 1–6, 2018.

[9] S. Loizou, "The navigation transformation," *IEEE Transactions on Robotics*, vol. 33, no. 6, pp. 1516–1523, 2017.

[10] E. Rimon and D. E. Koditschek, "Exact robot navigation using artificial potential functions," *IEEE International Journal of Robotics and Automation*, vol. 8, no. 5, pp. 501–518, 1992.

[11] A. J. van der Schaft and H. Schumacher, *An Introduction to Hybrid Dynamical Systems*. Springer, 2000.